Best Linear Time-Varying Approximation of a General Class of Nonlinear Time-Varying Systems

Hallemans, Noel; Pintelon, Rik; Van Gheem, Els; Collet, Thomas Marcel; Claessens, Raf; Wouters, Benny; Ramharter, Kristof ; Hubin, Annick; Lataire, John

Published in:
IEEE Transactions on Instrumentation and measurement

DOI:
10.1109/TIM.2021.3086891

Publication date:
2021

Document Version:
Accepted author manuscript

Best Linear Time-Varying Approximation of a General Class of Nonlinear Time-Varying Systems

Noël Hallemans, *Member, IEEE,* Rik Pintelon, *Fellow, IEEE,* Els Van Gheem, Thomas Collet, Raf Claessens, Benny Wouters, Kristof Ramharter, Annick Hubin and John Lataire, *Member, IEEE*

***Abstract*—This paper presents a method for estimating a linear time-varying approximation of a general class of nonlinear time-varying systems. It starts from noisy measurements of the response of the nonlinear time-varying system to a special class of periodic excitation signals. These measurements are subject to measurement noise, process noise and a trend.**

The proposed method is a two-step procedure. First, the disturbing noise variance is quantified. Next, using this knowledge, the linear time-varying dynamics are estimated together with the nonlinear time-varying distortions. The latter are split into even and odd contributions. As a result, the signal-to-nonlinear-distortion ratio is quantified. It allows one to decide whether or not a linear approximation is justifiable for the application at hand. The two-step algorithm is fully automatic in the sense that the user only has to choose upper bounds on the number of basis functions used for modeling the response signal.

The obtained linear time-varying approximation is the best in the sense that the difference between the actual nonlinear response and the response predicted by the linear approximation is uncorrelated with the input. Therefore, it is called the best linear time-varying approximation (BLTVA).

Finally, the theory is validated on a simulation example, and illustrated on two measurement examples: the cristallographic pitting corrosion of aluminum, and copper electrorefining.

***Index Terms*—odd random phase multisine, time-varying systems, nonlinear systems, time-varying frequency response function, even and odd nonlinear distortions, nonparametric estimation, trend**

I. Introduction

In many engineering applications, models of dynamical systems are needed, either for control, fault detection, physical insight, prototyping, prediction, or computer aided design. Initially, only linear time-invariant (LTI) systems were studied, owing to the rich and convenient system theoretic framework. Many types of models exist for this class of systems, including the impulse response function, the transfer function and the state space model. Moreover, mathematical relations transform one model into another, as each of them has particular pros and cons. Over the years, time- and frequency domain techniques were developed for identifying LTI systems [1] [2].

N. Hallemans, R. Pintelon and J. Lataire are with the department ELEC, Vrije Universiteit Brussel, 1050 Brussels, Noel.Hallemans@vub.be

E. Van Gheem is Project Leader at Infrax cvba, Heusden-Zolder, Belgium

A. Hubin, T. Collet, B. Wouters and R. Claessens are with the Research Group Electrochemical and Surface Engineering, Vrije Universiteit Brussel, 1050 Brussels

K. Ramharter is with Aurubis Belgium NV

This research was supported by the Fund for Scientific Research (FWO Vlaanderen), Flanders Innovation and Entrepreneurship (Baekeland grant HBC.2017.0212) and the Flemish Government (Methusalem Grant METH1).

In practice, the dynamics of very few real-life systems behave entirely linearly, and as a result, nonlinearities are introduced whenever the system is excited outside its linear operation region. These nonlinearities are among others present in measurements of RF amplifiers due to saturations [3], and in industrial robots with nonlinear dynamics with respect to the position [4]. Nonlinear time-invariant (NLTI) models do exist [5]. However, in many applications where the nonlinearities are not too strong, linear models are preferred as these are more simple to use. In response, the concept 'best linear approximation' was introduced in [6] and, next, generalized to the process noise case in [7] and [8].

Also, the system's dynamics are not always time-invariant. The joint impedance dynamics of the human body depend on time [9], and the impedance of a battery depends on the state-of-health and state-of-charge [10]. Thereupon, in frequency domain approaches, the concept of transfer function was extended to the time-varying transfer function (TV-TF); basically a transfer function that depends on time too [11]. In [12] a technique is detailed for estimating the TV-TF nonparametrically using basis functions as regressors, while in [13] Gaussian process regression is employed to model the time-variation. This last method has the advantage that the user interaction is reduced as a result of machine learning techniques. In both cases it is assumed that the system behaves linearly. Linear time-varying models have yet been applied in the chemical field for electrochemical impedance spectroscopy (EIS) [14] [15] [16] [17] [18].

As could be expected, it is also common that the system's dynamics behave both nonlinearly and in a time-varying way. An example is the pitting corrosion of aluminum immersed in an aerated sodium chloride solution [19]. Here, the best linear time-invariant model, under the form of a transfer function, was identified for the nonlinear time-varying (NLTV) process with the methods from [20]. The time-variation is detected via a difference in noise level between the excited and the non-excited frequencies. However, no direct quantification of the time-variation is made. As for today, techniques exist to model the time-variation of NLTV systems assuming that the nonlinearities are time-invariant. In [21] the time-varying transfer function is identified using a few periods of the transient response to a particular class of periodic excitation signals. However, that method cannot distinguish between even and odd nonlinear distortions and cannot handle trends in the data. The method of [22] solves both problems. Furthermore, it handles very wideband measurements and makes the user interaction simpler.

However, for real life systems, the time-invariance assumption on the nonlinearities does not always hold true. Eliminating the time-invariance assumption on the nonlinearity made in [22], is the main contribution of this paper. It requires a more general definition of the best linear time-varying approximation (BLTVA) introduced in [21]. As a result, from the transient response to a special class of periodic excitation signals, the BLTVA of a general class of time-varying nonlinear systems can be estimated together with the noise level and the level of the even and odd nonlinear distortions. Moreover, in contrast to [22], the even and odd nonlinear contributions can be split into a time-invariant and a time-varying part, and the impact of process noise on the results is analyzed.

The paper is organized as follows. First, we define the class $\mathbb{U}$ of periodic excitation signals and the class $\mathbb{S}$ of nonlinear systems considered (Section II). It includes an in-depth analysis of the spectral response of the class $\mathbb{S}$ to the class $\mathbb{U}$ of periodic inputs, and a study of the impact of process noise. Next, we handle the estimation of the disturbing noise variance (Section III), and the best linear time-varying approximation (Section IV) together with the even and odd nonlinear distortions (Section V). Using these results, the uncertainty calculation of the best linear time-varying approximation is elaborated (Section VI). Further, the proposed algorithm is validated on a simulated nonlinear time-varying system that satisfies the assumptions made (Section VII), and its performance is illustrated on measurements of crystallographic pitting corrosion (Section VIII) and copper electrorefining (Section IX). Finally, some conclusions are drawn in Section X.

II. Class of excitation signals and systems considered

A. Class of excitation signals considered

When identifying a system, the user has to decide on an appropriate excitation signal $u(t)$. Using a frequency domain approach, it is common to excite the system with a random phase multisine. Furthermore, when the system behaves nonlinearly, the following specially designed odd random phase multisines are used, which allows one to detect and quantify even and odd nonlinear distortions [22]:

Definition 1 (Class $\mathbb{U}$ of odd random phase multisines)**.** *$\mathbb{U}$ is the class of periodic excitation signals defined as*

$$u(t) = \sum_{k_e \in \mathbb{H}_{\text{exc}}} a_{k_e} \sin(\omega_{k_e} t + \varphi_{k_e}) \tag{1}$$

where $\mathbb{H}_{\text{exc}} \subset \mathbb{N}$ denotes the set of excited harmonics, $\omega_{k_e} = \frac{2\pi k_e}{T_p}$, T_p is the period of the multisine, $a_{k_e} \geqslant 0$ are the user-defined amplitudes and φ_{k_e} are independently (over k_e) uniformly distributed random phases $\in [0, 2\pi)$ such that $\mathbb{E}\{e^{j\varphi_{k_e}}\} = 0$.
The set of excited frequencies $\mathbb{H}_{\text{exc}}$ is chosen such that only odd harmonics are excited. It is constructed as follows. First, all odd harmonics in the frequency band of interest are generated. Next, these odd harmonics are grouped into L consecutive numbers, where $L > 1$. Finally, out of each group of L numbers, one randomly selected odd harmonic is eliminated.

For instance for $L = 5$, an example of the set $\mathbb{H}_{\text{exc}}$ in Definition 1 would be

$$\mathbb{H}_{\text{exc}} = \{1, 3, 5, 9, 11, 13, 17, 19, 21, 23, ...\}.$$

In practical measurements, sampled and windowed signals are available. Moreover, the discrete Fourier transform (DFT) is used to transform the signals into the frequency domain. The DFT of a signal $x(t)$ is defined as

$$X(k) = \frac{1}{N} \sum_{n=0}^{N-1} x(nT_{\text{s}}) e^{-j2\pi kn/N}, \tag{2}$$

where $k \in \mathbb{K} = \{0, 1, ..., N-1\}$ is the DFT bin, N is the number of time-domain samples, $T_{\text{s}} = 1/f_{\text{s}}$ is the sampling time, f_{s} is the sampling frequency and the measurement time is given by $T = NT_{\text{s}}$. In order to increase the frequency resolution f_{res} of the measurement, $f_{\text{res}} = 1/T$, with respect to the frequency resolution f_0 of the multisine, $f_0 = 1/T_p$, an integer number $P \gg 1$ of periods of the multisine are measured, such that the measurement time $T = PT_p$. Hence, the DFT (2) of P periods of $u(t)$ is only nonzero for the harmonics from the set

$$\mathbb{K}_{\text{exc}} = P\mathbb{H}_{\text{exc}}. \tag{3}$$

Increasing the frequency resolution of the measurement is beneficial for visualizing the time-variation in the output spectrum (see Section II-D) and contributes to the identifiability.

B. Class of nonlinear time-varying systems

To define the class of nonlinear time-varying systems considered, we must first recall some properties of the time-varying frequency response function.
For a certain time window $t \in [0, T]$, the input-output relation of continuous-time LTV systems can be written as [11]

$$y(t) = \mathcal{L}^{-1}\{G(s,t)U(s)\}, \tag{4}$$

where $y(t)$ is the output signal, $G(s,t)$ is called the time-varying transfer function (TV-TF) and $U(s)$ is the Laplace transform of the input signal $u(t)$. Note that this input-output relation is very similar to the one of an LTI system. However, here the transfer function also depends on the time. Identifying the LTV system boils down to obtaining the TV-TF $G(s,t)$. The series expansion of the TV-TF in a complete set of basis functions $b_p(t)$ gives

$$G(s,t) = \sum_{p=0}^{\infty} G_p(s) b_p(t). \tag{5}$$

Truncating this series

$$G(s,t) = \sum_{p=0}^{N_p} G_p(s) b_p(t) \tag{6}$$

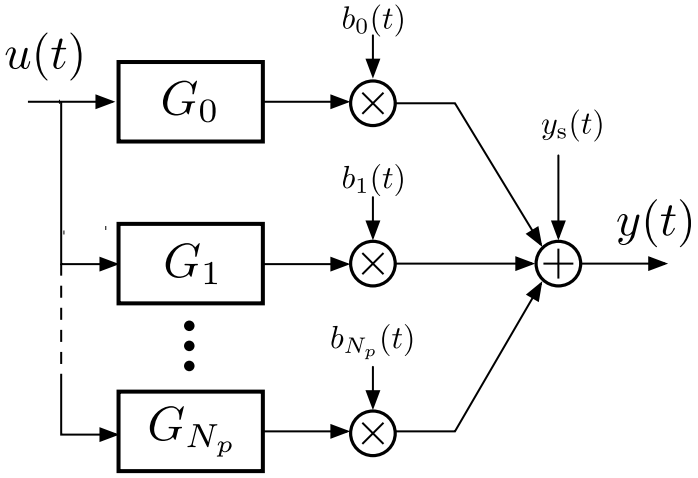

Fig. 1. Block schematic of LTV systems.

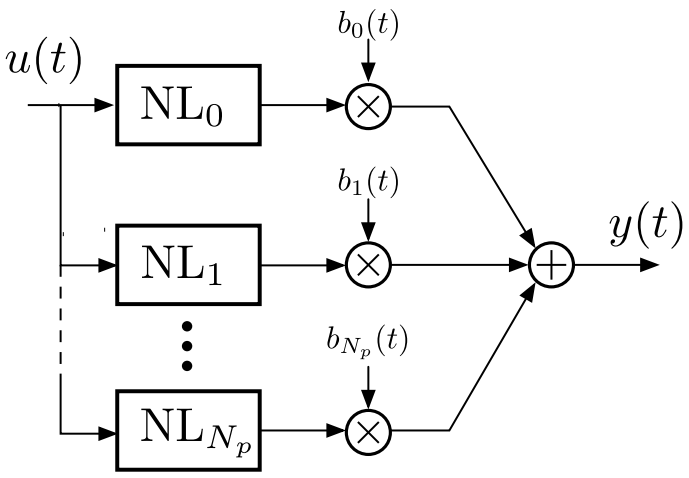

Fig. 2. Block schematic of the considered class of systems $\mathbb{S}$.

gives an arbitrarily good approximation for N_p sufficiently large. Combining the truncated series (6) with (4) results in the block diagram of Fig. 1 with $y_\mathrm{s}(t) = 0$,

$$y(t) = \sum_{p=0}^{N_p} \mathcal{L}^{-1}\{G_p(s)U(s)\}b_p(t). \tag{7}$$

In practice, the hyper parameter N_p is unknown beforehand, and is deduced from the data. For good numerical conditioning, Legendre polynomials are used as basis functions. These fulfill Legendre's differential equation,

$$\frac{\mathrm{d}}{\mathrm{d}x}\big((1-x^2)\frac{\mathrm{d}L_p(x)}{\mathrm{d}x}\big) + p(p+1)L_p(x) = 0 \quad x \in [-1,1] \tag{8}$$

and are rescaled over the measurement window $[0, T]$,

$$b_p(t) = L_p\left(\frac{2t}{T} - 1\right). \tag{9}$$

Moreover, the Legendre polynomials fulfill the conditions

$$b_0(t) = 1 \qquad \text{and} \qquad \frac{1}{T}\int_0^T b_p(t)\mathrm{d}t = 0 \quad \text{for } p \geq 1. \tag{10}$$

These properties will be exploited later on.

In this paper all the LTI blocks G_p are allowed to be NLTI systems, resulting in the block schematic of Fig. 2. The class of NLTI systems includes all systems whose response to the class $\mathbb{U}$ of input signals can be approximated arbitrary well in mean square sense by a Volterra series. The input-output relation of such a nonlinear block NL_p, illustrated in Fig. 3, yields

$$y_p(t) = \mathcal{L}^{-1}\{G_p(s)U(s)\} + y_{\mathrm{s},p}(t), \tag{11}$$

where $G_p(s)$ is the best linear approximation (BLA) of NL_p and $y_{\mathrm{s},p}(t)$ is a residual signal containing the nonlinear distortions [6]. Moreover these nonlinear distortions are uncorrelated with – but not independent of – the input $u(t)$, and can be split into the even and odd nonlinear contributions. These come respectively from the even and odd degree kernels in the Volterra series [2],

$$y_{\mathrm{s},p}(t) = y_{\mathrm{s,even},p}(t) + y_{\mathrm{s,odd},p}(t). \tag{12}$$

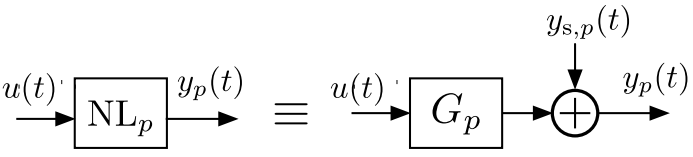

Fig. 3. Connection between an NLTI block and its BLA. $y_{\mathrm{s},p}(t)$ is uncorrelated with $u(t)$.

The algorithm presented in this paper allows us (i) to classify between the even and odd nonlinear distortions, and (ii) to distinguish the nonlinear contributions (12) of each branch in Fig. 2. Combining Figs. 2 and 3 yields Fig. 1, where

$$y(t) = \sum_{p=0}^{N_p} \mathcal{L}^{-1}\{G_p(s)U(s)\}b_p(t) + y_\mathrm{s}(t) \tag{13}$$

with

$$y_\mathrm{s}(t) = y_{\mathrm{s,even}}(t) + y_{\mathrm{s,odd}}(t), \tag{14}$$

$$y_{\mathrm{s,even}}(t) = \sum_{p=0}^{N_p} y_{\mathrm{s,even},p}(t)b_p(t). \tag{15}$$

and

$$y_{\mathrm{s,odd}}(t) = \sum_{p=0}^{N_p} y_{\mathrm{s,odd},p}(t)b_p(t). \tag{16}$$

Note that the nonlinear distortions $y_\mathrm{s}(t)$ of the system class $\mathbb{S}$ are the sum of amplitude modulated nonlinear distortions of NLTI systems. The considered class of systems and its best linear time-varying approximation (BLTVA) are now respectively formalized in Definitions 2 and 3.

Definition 2 (Class $\mathbb{S}$ of nonlinear time-varying systems)**.** *The considered class of systems $\mathbb{S}$ includes all nonlinear time-varying systems of which the input-output relationship can be written under the form of* (13)*, where $y_s(t)$ is given by* (14)*, and where $y_{s,p}(t)$ are the nonlinear distortions originating from an NLTI system whose response to the class $\mathbb{U}$ of input*

signals can be approximated arbitrary well in mean square sense by a Volterra series.

Note that this class of systems does not include all possible NLTV systems. Subharmonics, rate-independent hysteresis and chaos are, for instance, not covered. Still, it is shown to be a general class of NLTV systems as it works fine for different electrochemical processes, see the measurement examples in Sections VIII and IX.

Definition 3 (Best linear time-varying approximation)**.** *The best linear time-varying approximation of the class of systems* $\mathbb{S}$ *is given by the block schematic of Fig. 1 with* $y_{\text{s}}(t) = 0$*, where* G_p *is the BLA of NL*$_p$*. It is called the 'best' approximation as* $y_{\text{s},p}(t)$ (12) *is uncorrelated with – but not independent of –* $u(t)$*.*

In addition, a trend can be included by the proposed model structure. Different trend creating mechanisms are detailed in the Appendix. Furthermore, noise $n_y(t)$ is allowed in the measurement, resulting in the input-output relation

$$y(t) = y_{\text{trend}}(t) + \sum_{p=0}^{N_p} \mathcal{L}^{-1}\{G_p(s)U(s)\}b_p(t) + y_{\text{s}}(t) + n_y(t), \tag{17}$$

where the trend is modeled as

$$y_{\text{trend}}(t) = \sum_{q=0}^{N_q} \theta_q b_q(t). \tag{18}$$

The output noise signal $n_y(t)$ fulfills Assumption 1 [22].

Assumption 1 (Output noise)**.** *The disturbing noise signal* $n_y(t)$ *is assumed to be filtered band-limited white noise. Hence its DFT,* (2)*, can be written as*

$$N_y(k) = H(j\omega_k)E(k) + T_H(j\omega_k), \tag{19}$$

where $H(j\omega_k)$ *is a rational function of* $j\omega_k$ *representing the filtering operation,* $E(k)$ *is circular complex Gaussian distributed and uncorrelated over the frequency, and* $T_H(j\omega_k)$ *a rational function of* $j\omega_k$ *representing the noise transient.*

The output spectrum $Y(k)$ of the class of signals $\mathbb{S}$ is obtained by taking the DFT (2),

$$Y(k) = Y_{\text{trend}}(k) + Y_{\text{bltv}}(k) + T^{\circ}(j\omega_k) + Y_{\text{s}}(k) + V(k), \tag{20}$$

with $V(k) = H(j\omega_k)E(k)$ the noise contribution without the noise transient,

$$Y_{\text{trend}}(k) = \sum_{q=0}^{N_q} \theta_q B_q(k), \tag{21}$$

$$Y_{\text{bltv}}(k) = \sum_{p=0}^{N_p} G_p(j\omega_k)U(k) * B_p(k) \tag{22}$$

the output spectrum of the BLTVA of the system (Definition 3), where $*$ represents the convolution, $T^{\circ}(j\omega_k)$ the sum of the system and the noise transient, which is a smooth function of the frequency, and $Y_{\text{s}}(k)$ the nonlinear distortions that can be elaborated as

$$Y_{\text{s}}(k) = Y_{\text{s,even}}(k) + Y_{\text{s,odd}}(k) \tag{23}$$

with

$$Y_{\text{s,even}}(k) = \sum_{p=0}^{N_p} Y_{\text{s,even},p}(k) * B_p(k) \tag{24}$$

and

$$Y_{\text{s,odd}}(k) = \sum_{p=0}^{N_p} Y_{\text{s,odd},p}(k) * B_p(k). \tag{25}$$

Note that the spectra of the Legendre polynomials fulfill the following conditions due to properties (10),

$$B_0(0) = 1,\ B_0(k) = 0 \text{ for } k \neq 0 \text{ and } B_p(0) = 0 \text{ for } p \geq 1. \tag{26}$$

In practice the right hand side property is not entirely fulfilled because a finite number of samples are observed. Therefore, the mean values of the sampled and windowed $b_p(t)$ $p \geq 1$ are subtracted as in [22].

The objective of this paper is to identify the frequency response functions $G_p(j\omega_k)$ for $p = 0, 1, ..., N_p$ and $k \in \mathbb{K}_{\text{exc}}$, and to detect and quantify the disturbing noise level and the level of the even and odd nonlinear distortions in each branch of Fig. 2.

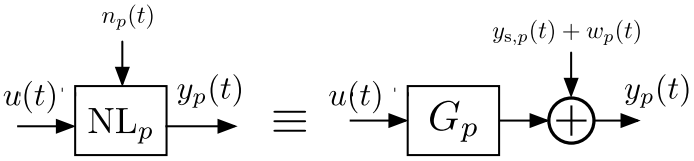

Fig. 4. Connection between an NLTI block with process noise and its BLA. $w_p(t)$ and $y_{\text{s},p}(t)$ are mutually uncorrelated and are uncorrelated with $u(t)$.

C. Impact of process noise

Real life measurements are not only subject to measurement noise, but also to process noise. This is noise generated by the system itself. The methods of this paper can be extended to the case of process noise. The process noise $n_p(t)$ acts on each nonlinear block NL$_p$, and the equivalence of Fig. 4 can then be stated [7], [8]. Hence, it holds that

$$y_p(t) = \mathcal{L}^{-1}\{G_p(s)U(s)\} + y_{\text{s},p}(t) + w_p(t), \tag{27}$$

where the nonlinear distortions $y_{\text{s},p}(t)$ and the process noise $w_p(t)$ of the block NL$_p$ are respectively defined as

$$y_{\text{s},p}(t) = \mathbb{E}\{y_p(t)|u(t)\} - \mathcal{L}^{-1}\{G_p(s)U(s)\} \tag{28}$$

and

$$w_p(t) = y_p(t) - \mathbb{E}\{y_p(t)|u(t)\}, \tag{29}$$

where $\mathbb{E}\{y_p(t)|u(t)\}$ is the expected value of $y_p(t)$ for a fixed input signal $u(t)$. The process noise $w_p(t)$ and the stochastic nonlinear distortions $y_{\text{s},p}(t)$ are mutually uncorrelated and are uncorrelated with – but not independent of – the input $u(t)$ [7],

[8]. Contrary to the linear case, $w_p(t)$ depends – in general – on the input $u(t)$. This is due to the nonlinear interactions between the input $u(t)$ and the noise $n_p(t)$ produced by the nonlinear system. Hence, changing the input rms value, can modify the variance of $w_p(t)$. The process noise of the total NLTV block schematic of Fig. 2 can then be written as

$$w(t) = \sum_{p=0}^{N_p} w_p(t) b_p(t). \tag{30}$$

Note that this process noise is non-stationary. Finally, the process noise can be added to the output noise $n_y(t)$ from Assumption 1, resulting in the noise signal

$$n'_y(t) = n_y(t) + w(t). \tag{31}$$

In Section III, a stationary approximation of the time-varying second order properties of (31) will be estimated.

D. Response of the class $\mathbb{S}$ of systems to the class $\mathbb{U}$ of inputs

With the choice of the odd random phase multisine from the class $\mathbb{U}$, the output spectrum $Y(k)$ (20) has a particular form.

For an odd multisine excitation (i.e. which excites only odd multiples of the fundamental frequency $f_0 = P/T$) the nonlinear distortions $y_{\text{s,even},p}(t)$ and $y_{\text{s,odd},p}(t)$ have only contributions at respectively even and odd multiples of the fundamental frequency, and hence at, respectively, the sets of harmonics [2]

$$\mathbb{K}_{\text{nl,even}} = \{0, 2P, 4P, ...\} \tag{32}$$

and

$$\mathbb{K}_{\text{nl,odd}} = \{P, 3P, 5P, ...\}. \tag{33}$$

Note that the set of excited harmonics is always a subset of $\mathbb{K}_{\text{nl,odd}}$. As $U(k)$, $Y_{\text{s,even},p}(k)$ and $Y_{\text{s,odd},p}(k)$ are thus only nonzero for, respectively, $k \in \mathbb{K}_{\text{exc}}$, $\mathbb{K}_{\text{nl,even}}$ and $\mathbb{K}_{\text{nl,odd}}$, the convolutions of (22), (24) and (25) are rewritten as follows,

$$Y_{\text{bltv}}(k) = \sum_{k' \in \mathbb{K}_{\text{exc}}} \sum_{p=0}^{N_p} G_p(j\omega_{k'}) U(k') B_p(k - k'), \tag{34}$$

$$Y_{\text{s,even}}(k) = \sum_{k' \in \mathbb{K}_{\text{nl,even}}} \sum_{p=0}^{N_p} Y_{\text{s,even},p}(k') B_p(k - k') \tag{35}$$

and

$$Y_{\text{s,odd}}(k) = \sum_{k' \in \mathbb{K}_{\text{nl,odd}}} \sum_{p=0}^{N_p} Y_{\text{s,odd},p}(k') B_p(k - k'). \tag{36}$$

It follows that the output spectrum $Y(k)$ (20) is given by the sum of scaled basis functions $B_p(k)$ – called skirts – centered around all the harmonics of the set

$$\mathbb{K}_{\text{nl}} = \{0, P, 2P, 3P, ...\}, \tag{37}$$

superposed by the transient term, which is a smooth function of the frequency, and the disturbing noise. An illustration of the input-output spectra of the system simulated in Section VII is shown at the top of Fig. 5, and a decomposed version with $Y_{\text{trend}}(k)$, $Y_{\text{bltv}}(k)$, $Y_{\text{s,even}}(k)$, $Y_{\text{s,odd}}(k)$ and $V(k)$ separately is shown in the bottom. Note that around the excited frequencies, $Y_{\text{bltv}}(k)$ and $Y_{\text{s,odd}}(k)$ have similar shapes and add up, making them undistinguishable from each other.

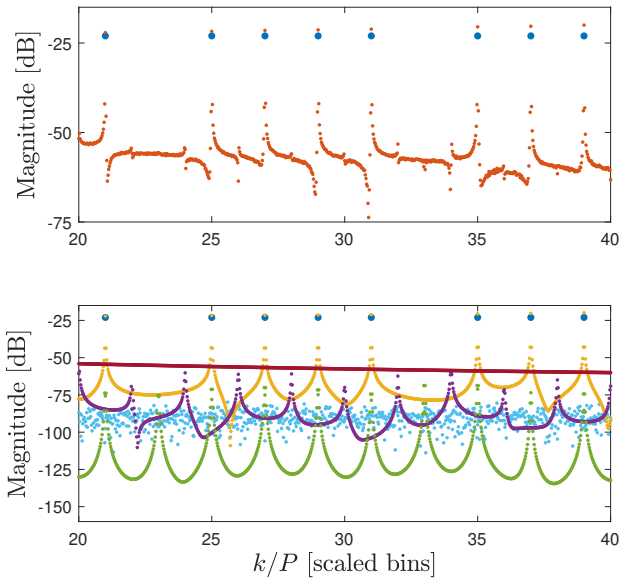

Fig. 5. Top: input-output spectra of a system belonging to the class $\mathbb{S}$ and excited by a signal from the class $\mathbb{U}$. Blue dots: $U(k)$ and red dots: $Y(k)$. Bottom: decomposed input-output spectra of a system from the class $\mathbb{S}$ excited by a signal from the class $\mathbb{U}$. Blue: $U(k)$, orange: $Y_{\text{bltv}}(k)$, purple: $Y_{\text{s,even}}(k)$, green: $Y_{\text{s,odd}}(k)$, bordeaux: $Y_{\text{trend}}(k)$ and light blue: $V(k)$. The system's parameters are detailed in the Section VII.

It will be explained in Section VII how $Y_{\text{bltv}}(k)$, $Y_{\text{s,even}}(k)$ and $Y_{\text{s,odd}}(k)$ were obtained from the simulation example.

It was discussed in [22] that a spectrum with skirts can be modeled by hyperbolas and polynomials. From these insights it will be possible to model the output spectrum, and to estimate the noise level from the residuals (Section III). In a next step, the TV-FRF is estimated together with its uncertainty due to the disturbing noise only and due to nonlinear distortions only.

III. Noise Estimation

The algorithm for estimating the noise is quite similar to the one in [22]. The difference is that skirts are fitted around all the integer multiples of the fundamental frequency instead of around the excited frequencies only. Moreover, as opposed to [22], the nonlinear distortions cannot be quantified in this step. The reason for this is that the algorithm automatically eliminates the redundant basis functions without identifying explicitly which basis functions are linearly independent. Here, the nonlinear distortions are quantified together with the time-varying FRF in the second step of the procedure (see Section V).

The noise estimation is done in a sliding frequency band, where the variable k_c runs over the entire band of interest. The band $\mathbb{K}_{\text{w}}$ is formed by taking $2n+1$ bins centered around

the bin k_c and removing the bins from the set $\mathbb{K}_{\text{nl}}$, i.e.

$$\begin{aligned}\mathbb{K}_{\text{w}} &= \{k_c - n, ..., k_c, ..., k_c + n\} \setminus \mathbb{K}_{\text{nl}} \\ &= \{k_1, k_2, ..., k_{N_{\text{w}}}\}. \end{aligned} \tag{38}$$

The data at the bins $\mathbb{K}_{\text{nl}}$ is disregarded because the model would not be able to distinguish between noise and dynamic behavior at these bins. The variable n is chosen based on the hyper parameter dof called the degrees of freedom which is set by default to 5,

$$n = \min\big(\text{ceil}\big(\frac{\text{dof} + n_{\theta,\max} + 2}{2}\big), P\big). \tag{39}$$

The maximal number of parameters to be estimated in this band is given by $n_{\theta,\max} = N_q + 3N_p + N_a + 1$ as at most 3 elements of $\mathbb{K}_{\text{nl}}$ can be comprised within the band (38). The value N_a is the degree of a polynomial used for modeling $T^{\circ}(j\omega_k)$. The data $Y(k)$ in this band is denoted as

$$Y_{\text{w}} = [Y(k_1), Y(k_2), ..., Y(k_{N_{\text{w}}})]^T. \tag{40}$$

The set of bins around which skirts could be present that have an influence on the band $\mathbb{K}_{\text{w}}$ is defined as

$$\mathbb{K}_{\text{nl,w}} = \mathbb{K}_{\text{nl}} \cap \{k_c - P, ..., k_c, ..., k_c + P\}, \tag{41}$$

and its cardinality is defined as $N_{\text{nl,w}}$. For $k \in \mathbb{K}_{\text{w}}$, the output spectrum $Y(k)$ can be modeled by the expression,

$$\begin{aligned}Y(k,\theta) = &\sum_{k' \in \mathbb{K}_{\text{nl,w}}} \sum_{p=1}^{N_p} \frac{\theta_p^{k'}}{(k-k')^p} + \sum_{q=1}^{N_q} \theta_q B_q(k) \\ &+ \sum_{r=0}^{N_a} \alpha_r L_r\big(2\frac{k-k_1}{k_{N_{\text{w}}} - k_1} - 1\big), \end{aligned} \tag{42}$$

where the first double sum models both $Y_{\text{bltv}}(k)$ and $Y_{\text{s}}(k)$, the second sum models $Y_{\text{trend}}(k)$ and the third sum models the sum of system and noise transient, and the parts of $Y_{\text{bltv}}(k)$ and $Y_{\text{s}}(k)$ that could not be modeled by the hyperbolas. This model can be rewritten in matrix notation,

$$Y_{\text{w}} = K\theta + V, \tag{43}$$

where Y_{w} is given by (40), K is a regression matrix consisting of the basis functions in (42), θ is a column vector with the $n_\theta = N_{\text{nl,w}}N_p + N_q + N_a + 1$ complex coefficients $\theta_p^{k'}$, θ_q and α_r, and $V \sim \mathcal{N}(0, C_V)$ with $C_V(k_l, k_m) = \sigma_V^2(k_l + k_1)\delta_{k_l,k_m}$. A least squares estimate of the output spectrum is then obtained as

$$\hat{Y}_{\text{w}} = K(K^H K)^{-1} K^H Y_{\text{w}}, \tag{44}$$

from which the residuals are computed,

$$\varepsilon = Y_{\text{w}} - \hat{Y}_{\text{w}} = (I - K(K^H K)^{-1} K^H) Y_{\text{w}}. \tag{45}$$

Using Theorem 1 of [22], the noise variance estimate at the bin k_c is calculated as,

$$\hat{\sigma}_V^2(k_c) = \frac{1}{N_{\text{w}} - m} \varepsilon_m^H \varepsilon_m, \tag{46}$$

where

$$\varepsilon_m = (I - U_m U_m^H) Y_{\text{w}}, \tag{47}$$

$$U_m = U \begin{bmatrix} I_m & 0 \\ 0 & 0 \end{bmatrix}, \tag{48}$$

U is an orthogonal matrix from the thin singular value decomposition of $K = U\Sigma W^H$ and I_m is the m by m identity matrix. How to obtain m is explained in Algorithm 1 which is strongly based on Algorithm 1 of [22]. The advantage of this algorithm is that the user only has to choose upper bounds on the hyper parameters N_p, N_q and N_a, because it automatically selects the significant linear independent basis functions in (42).

Guidelines for choosing the upper bounds on the hyper parameters N_p, N_q and N_a are included here. First of all, the total number of parameters is limited, as the number of equations should be higher than the number of parameters to be estimated. This results in the condition

$$n_{\theta,\max} < 2P - 1. \tag{49}$$

For practical measurements, good initial values are $P = 40$, $N_p = 10$, $N_q = 5$ and $N_a = 10$. The value N_a should be increased when the noise variance estimate is significantly higher in the valleys of the skirts as at the excited frequencies. The value N_p should be increased as long as there is correlation over the frequency in the residual vector ε. The value N_q can be chosen from the time-domain output signal. Note that when (49) does not hold anymore, one should redo the measurement with a higher number of periods.

Algorithm 1 Noise variance estimation

For each k_c in $\mathbb{K}$

Step 1:

1) Take the data Y_{w} (40) in the band $\mathbb{K}_{\text{w}}$ (38) and form the corresponding regression matrix K.
2) Compute $\Sigma = \text{diag}([\sigma_1, \sigma_2, ..., \sigma_{n_\theta}])$ which is the matrix of singular values of K in decreasing order, i.e. $\sigma_i > \sigma_{i+1}$.
3) Compute
$$l = \min_i i \text{ s.t.} \frac{\sigma_{i+1}}{\sigma_1} < 10^{-10}. \tag{50}$$
4) Compute a first estimate of the noise variance from (47)
$$\hat{\sigma}_V^2 = \frac{1}{N_{\text{w}} - l} \varepsilon_l^H \varepsilon_l \tag{51}$$

Step 2:

1) Compute the snr in the band
$$\text{snr} = \sqrt{\frac{Y_{\text{w}}^H Y_{\text{w}}}{N_{\text{w}} \hat{\sigma}_V^2}} \tag{52}$$
2) Compute
$$m = \min_i i \text{ s.t.} \frac{\sigma_{i+1}}{\sigma_1} < a \text{ snr}, \tag{53}$$
where $a = 10$ is a safety factor.
3) Compute the estimate of the noise variance,
$$\hat{\sigma}_V^2(k_c) = \frac{1}{N_{\text{w}} - m} \varepsilon_m^H \varepsilon_m. \tag{54}$$

IV. Estimation of the TV-FRF

The model estimation is also performed in a sliding window algorithm where the variable k_e runs over all elements of the set $\mathbb{K}_{\text{exc}}$. A band comprising three consecutive excited frequencies, k_e^-, k_e, k_e^+, is then formed as

$$\begin{aligned}\mathbb{K}_{\text{w}} &= \{k_e^- - \Delta k_e^-, ..., k_e^-, ..., k_e, ..., k_e^+, ..., k_e^+ + \Delta k_e^+\} \\ &= \{k_1, k_2, ..., k_{N_{\text{w}}}\},\end{aligned} \tag{55}$$

where Δk_e^- and Δk_e^+ are half the distances in bins to, respectively, the previous and the next excited bins outside the window. Note that here all data is used, as opposed to the noise estimation. The data at the bins $\mathbb{K}_{\text{w}}$ is denoted as

$$Y_{\text{w}} = [Y(k_1), Y(k_2), ..., Y(k_{N_{\text{w}}})]^T. \tag{56}$$

Note the double use of notation with respect to (40). However, both are defined over different frequency bands and, hence, are distinct. The set

$$\mathbb{K}_{\text{nl,w}} = \mathbb{K}_{\text{w}} \cap \mathbb{K}_{\text{nl}} \setminus k_e \tag{57}$$

contains all bins in the band, except k_e, around which skirts could be present. Define $N_{\text{nl,w}}$ as the cardinality of $\mathbb{K}_{\text{nl,w}}$. The data in the band can then be modeled as

$$\begin{aligned}Y(k,\theta) = &\sum_{p=0}^{N_p} \theta_p(k_e) B_p(k-k_e) + \sum_{k' \in \mathbb{K}_{\text{nl,w}}} \sum_{p=0}^{N_p} \theta_p(k') B_p(k-k') \\ &+ \sum_{q=0}^{N_q} \theta_q B_q(k) + \sum_{r=0}^{N_a} \alpha_r L_r\big(2\frac{k-k_1}{k_{N_{\text{w}}} - k_1} - 1\big),\end{aligned} \tag{58}$$

where

$$\theta_p(k_e) = G_p(j\omega_{k_e}) U(k_e) + Y_{\text{s,odd},p}(k_e), \tag{59}$$

$$\theta_p(k') = Y_{\text{s,even},p}(k') \tag{60}$$

for $k' \in \mathbb{K}_{\text{nl,even}}$, and

$$\theta_p(k') = G_p(j\omega_{k'}) U(k') + Y_{\text{s,odd},p}(k') \tag{61}$$

for $k' \in \mathbb{K}_{\text{nl,odd}} \setminus k_e$, where $U(k') = 0$ for $k' \in \mathbb{K}_{\text{nl,odd}} \setminus \mathbb{K}_{\text{exc}}$. The first sum in (58) models both the time-variation and nonlinearities at the middle excited bin, the second double sum models the remaining of $Y_{\text{bltv}}(k)$ and $Y_{\text{s}}(k)$, the third sum models $Y_{\text{trend}}(k)$, and the fourth term models $T^{\circ}(j\omega_k)$. Note that the time-varying and the nonlinear behavior are undistinguishable at the middle excited bin and, hence, grouped in (59). From this model of the output spectrum, we identify the coefficients $G_p(j\omega_{k_e})$, $p = 0, 1, ..., N_p$. Note that the same values for the hyper parameters N_p, N_q and N_a are chosen as in Section III.

Again, a matrix equality can be formed,

$$Y_{\text{w}} = K\theta + V, \tag{62}$$

where K is the regression matrix, see Algorithm 2, and θ contains the coefficients $\theta_p(k_e)$, $\theta_p(k')$, θ_q and α_r. These parameters can be estimated in least squares sense from the data Y_{w} using Algorithm 2. This algorithm is quite similar to Algorithm 2 in [22]. However, in its present form, skirts are fitted around all integer multiples of the fundamental frequency, and only the significant basis functions are retained. This algorithm first removes those polynomials that depend linearly on the functions B_p. Next, it selects the basis functions B_p with a contribution – at least at one frequency – above the noise level. Finally, a least squares estimate of the parameters θ is computed. From $\hat{\theta}$, the estimates $\hat{G}_p(j\omega_{k_e})$, $p = 0, ..., N_p$ are retained. These estimates are affected by the terms $Y_{\text{s,odd},p}(k_e)$ and $V(k)$. The uncertainty due to these terms is handled in Section VI. Finally the estimate of the BLTVA yields, for $k \in \mathbb{K}_{\text{exc}}$,

$$\hat{G}(j\omega_k, t) = \sum_{p=0}^{N_p} \hat{G}_p(j\omega_k) b_p(t). \tag{63}$$

V. Nonlinear distortions estimation

In Section IV we identified the level of the even and odd nonlinear distortions in each branch of the block diagram of Fig. 2. From these values we can estimate the variance of the nonlinear distortions at the nonlinear harmonics. To estimate the variance at the excited frequencies we take an average of the variances at the nearest odd nonlinear harmonics left and right from the excited one. Proceeding in this way we get:

$$\hat{\sigma}^2_{Y_{\text{s,class},p}}(k) = \begin{cases} \max\big(\sigma^2_{\text{tmp,class},0}(k) - \hat{\sigma}^2_V(k), 0\big) \text{ for } p = 0 \\ \sigma^2_{\text{tmp,class},p}(k) \text{ for } p \geqslant 1, \end{cases} \tag{69}$$

where class is either even or odd,

$$\sigma^2_{\text{tmp,even},p}(k) = |\hat{Y}_{\text{s,even},p}(k)|^2 \text{ for } k \in \mathbb{K}_{\text{nl,even}} \tag{70}$$

and

$$\sigma^2_{\text{tmp,odd},p}(k) = \begin{cases} |\hat{Y}_{\text{s,odd},p}(k)|^2 \text{ for } k \in \mathbb{K}_{\text{nl,odd}} \setminus \mathbb{K}_{\text{exc}} \\ \frac{1}{2}\big(|\hat{Y}_{\text{s,odd},p}(k^-)|^2 + |\hat{Y}_{\text{s,odd},p}(k^+)|^2\big) \text{ for } k \in \mathbb{K}_{\text{exc}}, \end{cases} \tag{71}$$

with k^- and k^+ respectively the closest bins left and right from k belonging to the set $\mathbb{K}_{\text{nl,odd}} \setminus \mathbb{K}_{\text{exc}}$. The indices are taken from the set $\mathbb{K}_{\text{nl,odd}}$, as only odd nonlinear distortions can be centered around the excited frequencies.

From the levels of $\hat{\sigma}^2_{Y_{\text{s,even}},p}(k)$ and $\hat{\sigma}^2_{Y_{\text{s,odd}},p}(k)$ with respect to $|Y(k)|^2$ at the excited frequencies, one can decide whether the linear approximation of the system is acceptable or not for a certain application.

VI. Uncertainty estimation

The TV-FRF (63) is computed from data corrupted by nonlinear distortions and (process) noise. Unfortunately, one cannot always discriminate between the nonlinear distortions $Y_{\text{s}}(k)$ and the best linear time-varying output spectrum $Y_{\text{bltv}}(k)$. The skirts created by nonlinear distortions are summed to the linear output spectrum around the excited frequencies, and both cannot be distinguished. Hence, uncertainties are introduced in the estimated TV-FRF. In this section the problem is addressed via the total variance on the TV-FRF, which is the variance due to the noise and the nonlinear distortions.

Consider again the sliding window algorithm of Section IV.

Algorithm 2 Signal model estimation

For each k_e in $\mathbb{K}_{\text{exc}}$

1) Compute the band $\mathbb{K}_{\text{w}}$ (55) and consider the data Y_{w} (56) in this band.
2) Form the regression matrix K, with in the first N_p+1 columns the regressors $B_p(k-k_e)$, in the next $N_{\text{nl,w}}(N_p+1)$ columns the regressors $B_p(k)$ centered around $\mathbb{K}_{\text{nl,w}}$, in the next N_q+1 columns the regressors $B_q(k)$ centered around DC and, finally, in the last N_a+1 columns the polynomials $L_r(2\frac{k-k_1}{k_{N_{\text{w}}}-k_1}-1)$
3) Determine the transient order:
   For $d = N_a, N_a-1, ..., 1$
   - compute the thin SVD of K.
   - compute
   $$l_d = \arg\min_i \frac{\sigma_i}{\sigma_1} > 10^{-10}.$$
   - if $l_d \leq l_{d-1}-1$: end loop.
     else: remove the last column of K.
4) Compute the parameters
   $$\hat{\theta} = K^+ Y_{\text{w}}. \tag{64}$$
5) Compute the mean value of the noise variance estimates (46) in the band
   $$\sigma_n^2 = \text{mean}\big([\hat{\sigma}_V^2(k_1), \hat{\sigma}_V^2(k_2), ..., \hat{\sigma}_V^2(k_{N_{\text{w}}})]\big). \tag{65}$$
6) for $r = (N_{\text{nl,w}}+1)(N_p+1)+N_q+1, ..., 1$
   - compute
   $$a_r = \max_i \big(|\hat{\theta}_{[r]}|^2 |K_{[i,r]}|^2\big) \tag{66}$$
   where $K_{[i,r]}$ denotes the element on the i-th row and r-th column of K and $\hat{\theta}_{[r]}$ the r-th element of $\hat{\theta}$.
   - if $a_r < 3\sigma_n^2$ (95 % confidence bound): remove the r-th column of K.
7) Recompute the parameters with the new regression matrix K,
   $$\hat{\theta} = K^+ Y_{\text{w}}. \tag{67}$$
8) Obtain the estimates
   $$\hat{G}_p(j\omega_{k_e}) = \frac{\hat{\theta}_{[p]}}{U(k_e)} \qquad \text{for } p = 0, 1, ..., N_p, \tag{68}$$
   where the ones that were not identified due to the reduction of the number of basis functions are set to zero.
9) Also retain the coefficients corresponding to $\hat{Y}_{\text{s,even},p}(k)$ for $k \in \mathbb{K}_{\text{nl,even}}$ and $\hat{Y}_{\text{s,odd},p}(k)$ for $k \in \mathbb{K}_{\text{nl,odd}} \setminus \mathbb{K}_{\text{exc}}$ from $\hat{\theta}$.

The parameters of the model $\hat{\theta}$ for the band $\mathbb{K}_{\text{w}}$ (55) are computed via a pseudoinverse (64). The noise covariance of these estimated parameters is then given by

$$C_{\hat{\theta}} = \text{cov}\{\hat{\theta}\} = K^+ C_V K^{+H}, \tag{72}$$

where C_V is the covariance matrix of the noise in the band (55), which is very simply formed as

$$C_V = \text{diag}\big([\sigma_V^2(k_1), \sigma_V^2(k_2), ..., \sigma_V^2(k_{N_{\text{w}}})]\big), \tag{73}$$

where $\sigma_V^2(k)$ is obtained from (46).
Remember that the estimates $\hat{G}_p(j\omega_{k_e})$ are given by (68) where

$$\theta_{[p]} = G_p(j\omega_{k_e})U(k_e) + Y_{\text{s,odd},p}(k_e). \tag{74}$$

Note that only the noise (31) and the odd nonlinear distortions have an impact on the uncertainties of $\hat{G}_p(j\omega_{k_e})$. Both are uncorrelated and, hence, for

$$\overline{G}(j\omega_{k_e}) = [\hat{G}_0(j\omega_{k_e}), \hat{G}_1(j\omega_{k_e}), ..., \hat{G}_{N_p}(j\omega_{k_e})]^T, \tag{75}$$

one finds that,

$$C_{\overline{G}}(j\omega_{k_e}) = \text{cov}\{\overline{G}(j\omega_{k_e})\} = \frac{C_{\overline{\theta}} + C_{\overline{Y}_{\text{s,odd}}}}{|U(k_e)|^2}. \tag{76}$$

Here, one has that

$$C_{\overline{\theta}} = C_{\hat{\theta}[1:N_p+1, 1:N_p+1]}, \tag{77}$$

where MATLAB notation has been used for the indices and $C_{\hat{\theta}}$ is given by (72). Further, $C_{\overline{Y}_{\text{s,odd}}} = \text{cov}\{\overline{Y}_{\text{s,odd}}\}$, with

$$\overline{Y}_{\text{s,odd}} = [Y_{\text{s,odd},0}(k_e), Y_{\text{s,odd},1}(k_e), ..., Y_{\text{s,odd},N_p}(k_e)]^T. \tag{78}$$

Since $\overline{Y}_{\text{s,odd}}$ is unknown, $C_{\overline{Y}_{\text{s,odd}}}$ is approximated as

$$C_{\overline{Y}_{\text{s,odd}}} \approx \frac{1}{2}\big(\overline{Y}^-_{\text{s,odd}}\overline{Y}^{-H}_{\text{s,odd}} - B_l^+ C_V B_l^{+H} + \overline{Y}^+_{\text{s,odd}}\overline{Y}^{+H}_{\text{s,odd}} - B_r^+ C_V B_r^{+H}\big), \tag{79}$$

with B_l and B_r $N_{\text{w}} \times N_p+1$ matrices

$$B_l = \begin{bmatrix} B_0(\mathbb{K}_{\text{w}}-k^-) & B_1(\mathbb{K}_{\text{w}}-k^-) & \dots & B_{N_p}(\mathbb{K}_{\text{w}}-k^-) \end{bmatrix}, \tag{80}$$

$$B_r = \begin{bmatrix} B_0(\mathbb{K}_{\text{w}}-k^+) & B_1(\mathbb{K}_{\text{w}}-k^+) & \dots & B_{N_p}(\mathbb{K}_{\text{w}}-k^+) \end{bmatrix}, \tag{81}$$

$$\overline{Y}^-_{\text{s,odd}} = [\hat{Y}_{\text{s,odd},0}(k^-), \hat{Y}_{\text{s,odd},1}(k^-), ..., \hat{Y}_{\text{s,odd},N_p}(k^-)]^T \tag{82}$$

and

$$\overline{Y}^+_{\text{s,odd}} = [\hat{Y}_{\text{s,odd},0}(k^+), \hat{Y}_{\text{s,odd},1}(k^+), ..., \hat{Y}_{\text{s,odd},N_p}(k^+)]^T, \tag{83}$$

and where k^- and k^+ are respectively the closest harmonics left and right from k_e that belong to the set $\mathbb{K}_{\text{nl,odd}} \setminus \mathbb{K}_{\text{exc}}$. The coefficients $\hat{Y}_{\text{s,odd},p}$ are found from the last step in Algorithm 2. Note that the noise variance has been removed from the nonlinear distortion variances. Moreover, the covariances of $\overline{G}(j\omega_{k_e})$ due to nonlinear distortions only, and due to noise only are, respectively,

$$C_{\overline{G},Y_{\text{s}}}(j\omega_{k_e}) = \frac{C_{\overline{Y}_{\text{s,odd}}}}{|U(k_e)|^2} \text{ and } C_{\overline{G},V}(j\omega_{k_e}) = \frac{C_{\overline{\theta}}}{|U(k_e)|^2}. \tag{84}$$

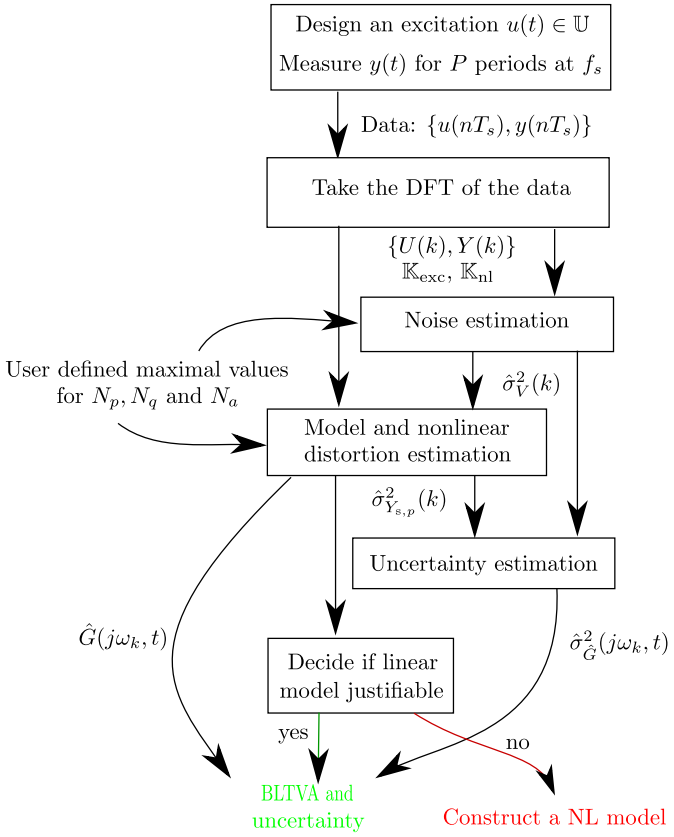

Fig. 6. Flowchart of the complete modelling procedure. $\mathbb{K}_{\text{exc}}$ is defined in (3), $\mathbb{K}_{\text{nl}}$ in (37), the noise variances $\hat{\sigma}^2_V(k)$ in (46), the nonlinear distortion variances $\hat{\sigma}^2_{Y_{s,p}}(k)$ in (69), the BLTVA $\hat{G}(j\omega_k, t)$ in (63) and its variance $\hat{\sigma}^2_{\hat{G}}(j\omega_k, t)$ in (87).

Finally, since the TV-FRF can be written as

$$\hat{G}(j\omega_{k_e}, t) = \overline{b}(t)\overline{G}(j\omega_{k_e}), \tag{85}$$

where

$$\overline{b}(t) = [b_0(t), b_1(t), ..., b_{N_p}(t)], \tag{86}$$

the total variance of the estimated TV-FRF is given by

$$\hat{\sigma}^2_{\hat{G}}(j\omega_{k_e}, t) = \overline{b}(t) C_{\overline{G}}(j\omega_{k_e}) \overline{b}^T(t). \tag{87}$$

Similarly, we find for the variance caused by nonlinear distortions

$$\hat{\sigma}^2_{\hat{G},Y_s}(j\omega_{k_e}, t) = \overline{b}(t) C_{\overline{G},Y_s}(j\omega_{k_e}) \overline{b}^T(t) \tag{88}$$

and for the variance caused by noise

$$\hat{\sigma}^2_{\hat{G},V}(j\omega_{k_e}, t) = \overline{b}(t) C_{\overline{G},V}(j\omega_{k_e}) \overline{b}^T(t). \tag{89}$$

As a summary, a flow chart of the complete modelling procedure for obtaining an estimate of the BLTVA $\hat{G}(j\omega_{k_e}, t)$ and its uncertainty $\hat{\sigma}^2_{\hat{G}}(j\omega_{k_e}, t)$ is given in Fig. 6.

VII. Simulation Example

The identification methodology of this paper is validated by 100 Monte-Carlo runs on a system satisfying Definition 2 (see Fig. 2 with $N_p = 2$), corrupted by a trend and additive noise at the output. The input signal $u(t)$ is an odd random phase multisine (see Definition 1) of $1\,\text{V}_{\text{rms}}$ with a period length $T_p = 100\,\text{s}$ and $L = 5$. Each nonlinear block NL_p of the system is given by a block schematic as in Fig. 7, where $H_p(s)$ is an LTI dynamic system and $f^1_p(x)$ and $f^2_p(x)$ are static nonlinear functions.

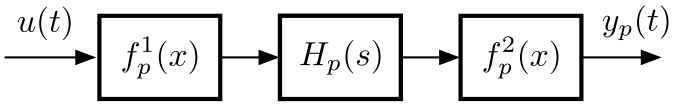

Fig. 7. Simulated nonlinear blocks NL_p.

The simulated system is defined by the following input-output relation,

$$y(t) = y_{\text{trend}}(t) + y_{\text{block}}(t) + v(t) \tag{90}$$

where

$$y_{\text{trend}}(t) = 5b_1(t) + 3b_2(t), \tag{91a}$$

$$y_{\text{block}}(t) = \sum_{p=0}^{N_p} y_p(t) b_p(t), \tag{91b}$$

$$y_p(t) = f^2_p\big(\mathcal{L}^{-1}\{H_p(s)\mathcal{L}\{f^1_p(u(t))\}\}\big), \tag{91c}$$

$$f^1_0(x) = x + 0.02\tanh(x-2), \tag{91d}$$

$$f^2_0(x) = x + 0.03\tanh(x-1), \tag{91e}$$

$$f^1_1(x) = x + 0.08x^2, \quad f^2_1(x) = x, \tag{91f}$$

$$f^1_2(x) = x, \quad f^2_2(x) = x + 0.15x^3, \tag{91g}$$

and

$$v(t) \sim \mathcal{N}(0, \sigma^2_v). \tag{91h}$$

Furthermore, $H_0(s)$, $H_1(s)$ and $H_2(s)$ are second order filters (all zeros at infinity) with natural frequencies $\omega_{n,0} = 0.7\,\text{Hz}$, $\omega_{n,1} = 1\,\text{Hz}$, $\omega_{n,2} = 1.5\,\text{Hz}$, damping ratios $\zeta_0 = 0.15$, $\zeta_1 = 0.1$ and $\zeta_2 = 0.15$, and DC gains $H_0(0) = 1$, $H_1(0) = 0.2$ and $H_2(0) = 0.2$, and $\sigma_v = 0.005$. The signal-to-noise ratio is equal to 342. Note that NL_0 is a Wiener-Hammerstein system, NL_1 a Hammerstein system and NL_2 a Wiener system.

The signals $u(t)$ and $y(t)$ are measured for $P = 40$ periods at a sampling rate $f_s = 20\,\text{Hz}$, resulting in a measurement time of $T = 4000\,\text{s}$ and $N = 80000$ data points.

The procedures of Sections III-VI are applied to the simulated data with the following upper bounds on the hyper parameters in (42) and (58): $N_p = 8$, $N_a = 10$, $N_q = 5$ and $\text{dof} = 5$. With these choices, the local bandwidth in step 1 (Section III) equals $2n + 1 = 45$ (0.0112 Hz). For the noise estimation, the number of nonzero singular values m, varies over the frequency between 11 and 24 while $n_\theta = 32$ or 40, depending on the local frequency band. From Fig. 8, one notices that the noise variance has been estimated correctly. In Fig. 9 the

variances of the nonlinearities are shown. They are correctly detected, quantified and classified. In agreement with (91d), (91e), (91f) and (91g) the time-invariant branch contains both even and odd nonlinear distortions, the branch $p = 1$ only even ones and the branch $p = 2$ only odd ones. The variances of the nonlinear distortions are at least 20 dB smaller than the linear part of the measurement. Hence, with this knowledge the user can determine whether a linear model is justifiable, depending on the application. Note that the true even nonlinear distortion variances have a contribution at DC, despite the fact that DC is not excited in the simulation. When NL_p has even nonlinear contributions, excited frequencies are folded back to DC.

The true values of $Y_{\text{s,even},p}(k)$ and $Y_{\text{s,odd},p}(k)$ were obtained as follows. For each nonlinear block NL_p the BLA $G_p(s)$ is computed by averaging the ratio $Y(k)/U(k)$, with $k \in \mathbb{K}_{\text{exc}}$, over 100 different random phase realizations of the input signal. Then $Y_{\text{s},p}(k) = Y(k) - G_p(j\omega_k)U(k)$ is computed, and further the variances of $Y_{\text{s,even},p}(k)$ and $Y_{\text{s,odd},p}(k)$.

The estimated block schematic FRFs $G_p(j\omega_{k_e})$ and their covariances $C_{\overline{G}}(j\omega_{k_e})$ and $C_{\overline{G},V}(j\omega_{k_e})$ are shown in Fig. 10. Note that while the user asks for maximal $N_p + 1 = 9$ LTI blocks, only 3 blocks are selected by the procedure of Section IV, which is in agreement with the actual simulated system. For validating the uncertainties, we compare the sample variance over the 100 estimates to the mean value of the estimated total variances. The total variances on each of the branches of the block structure were identified correctly as they coincide within the 95% uncertainty bounds of the Monte-Carlo simulation. Note that the variance on G_1 due to nonlinear distortions is zero, as in this branch the nonlinear distortions are purely even, and hence introduce no uncertainty on the BLA.

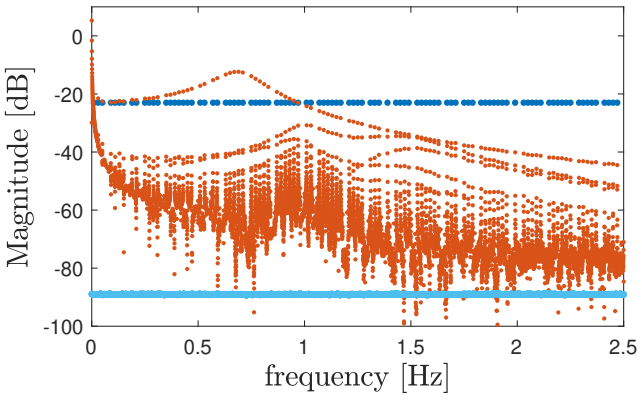

Fig. 8. Input-output spectrum of the simulation. Blue: $U(f)$, red: $Y(f)$ and light blue: mean value of the estimated noise variances $\hat{\sigma}^2_V(f)$ over 100 random phase realizations of the multisine. Note that the estimated noise variances lay on top of the true noise variance $\sigma^2_V = -89$ dB.

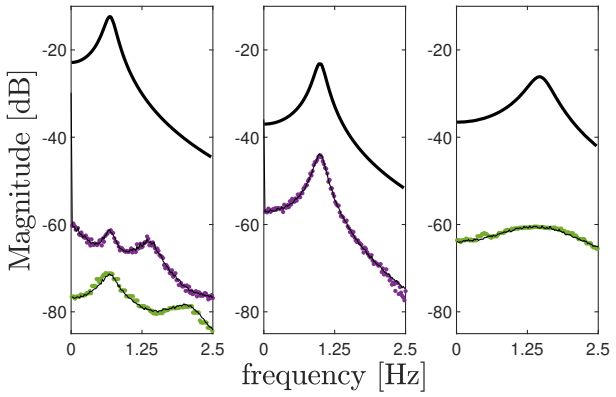

Fig. 9. Monte-Carlo simulation for 100 random phase realizations of the multisine. Black: $G_p(j2\pi f)U(f)$, purple: $\sigma^2_{Y_{\text{s,even},p}}(f)$, green: $\sigma^2_{Y_{\text{s,odd},p}}(f)$ (full line: true values, dots: mean of estimated values). Left: $p = 0$, middle: $p = 1$ and right $p = 2$.

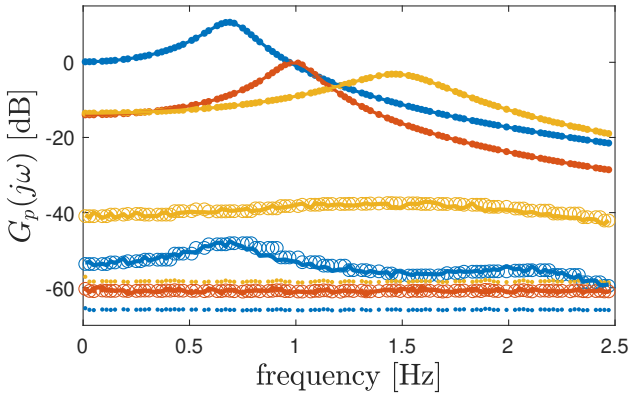

Fig. 10. Monte-Carlo (MC) simulation for 100 random phase realizations of the multisine. The true BLA's of the simulation (upper full lines) coincide with the mean values of the estimated BLA's (dots). The sample variances of the estimated BLA's (lower full lines) coincide with the mean value of the estimated total variances (circles). These total variances lie well above the estimated noise variances (dots). Blue: $p = 0$, red: $p = 1$ and yellow: $p = 2$.)

VIII. Measurement Example I

The method described in this paper is now applied to measurements of crystallographic pitting corrosion of aluminum. The objective is to estimate the time-varying admittance of the aluminum during a corrosion process. This is done by imposing a voltage to the system and measuring the current response. The chemical information about the aluminum sample and the corrosion process is detailed in Section 2 of [19]. The excitation signal is the open circuit potential of 797 mV superimposed by an odd random phase multisine of 15 mV_{rms}, exciting 179 frequencies in the band $[19\,\text{mHz}, 24\,\text{Hz}]$ and with a period length $T_p = 52\,\text{s}$. Both current and voltage signals were measured for $P = 121$ periods of the multisine signal, corresponding to a measurement time $T = 6344\,\text{s}$, at a sampling rate $f_s = 5\,\text{kHz}$. The input-output spectrum is shown in Fig. 11. From the decreasing spectrum at the very low frequencies, one notices that a trend is present. The methods from this paper are applied with hyper parameters

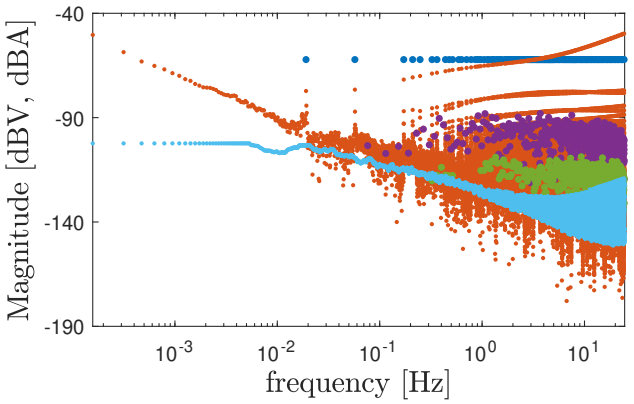

Fig. 11. Input-output spectrum of the system. Blue: $U(f)$, red: $Y(f)$, purple: $\hat{\sigma}^2_{Y_{\mathrm{s,even},0}}(f)$, green: $\hat{\sigma}^2_{Y_{\mathrm{s,odd},0}}(f)$ and light blue: $\hat{\sigma}^2_V(f)$.

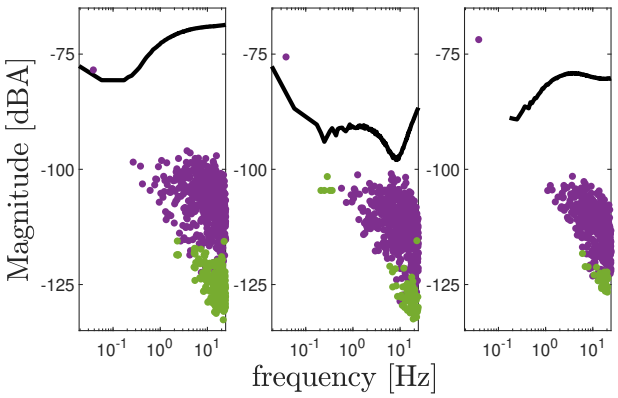

Fig. 12. Estimated nonlinear distortion variances for the three first blocks. Black: $\hat{G}_p(j2\pi f)U(f)$, purple: $\sigma^2_{Y_{\mathrm{s,even},p}}(f)$, green: $\sigma^2_{Y_{\mathrm{s,odd},p}}(f)$. Left: $p = 1$, middle: $p = 2$ and right $p = 3$.

$N_q = 5$, $N_p = 10$, $N_a = 10$ and $\mathrm{dof} = 5$ in (42) and (58). This results in a local bandwidth of $2n + 1 = 51$ (8 mHz). For the noise estimation, the number of nonzero singular values m varies over the frequency between 11 and 17 while $n_\theta = 36$ or 46. The estimates of the even and odd stationary nonlinear distortions, and the noise level are shown in Fig. 11. The estimates of the nonlinear distortions of the three first time-varying branches are shown in Fig. 12. Even and odd nonlinear distortions are detected, quantified and classified, and it can be seen that the even ones are the most dominant for all the branches shown. Still, a minimal signal-to-nonlinear-distortion ratio of 30 dB is guaranteed on the time-invariant branch, which increases fastly over frequency. Hence a linear model could be justifiable. A zoomed version of the input-output spectrum is shown in Fig. 13. Here it is clearly visible that skirts are present around all integer multiples of the fundamental frequency $f_0 = 19$ mHz, and, hence, time-varying nonlinearities are present. Note that the noise estimate is higher around the excited frequencies. It can be proven, by increasing N_p and N_a, that the residuals become totally white, while the higher noise estimate around the excited frequencies stays. Thus, this phenomena could not be explained by undermodeling. Hence, it must be due to nonlinear process noise – input signal interactions in the pitting corrosion dynamics. In Fig. 14 the same window is shown, but identified with the method of [22]. Here, the noise estimate is higher around the integer multiples of the fundamental frequency, showing that the method fails in the presence of time-varying nonlinear distortions.

The LTI transfer function blocks are shown in Fig. 15 together with their uncertainties due to noise, nonlinear distortions and both. Finally the time-varying admittance of the corroding aluminum is shown in Figs. 16 and 17. The uncertainties of the time-varying admittance are not shown for reasons of clarity.

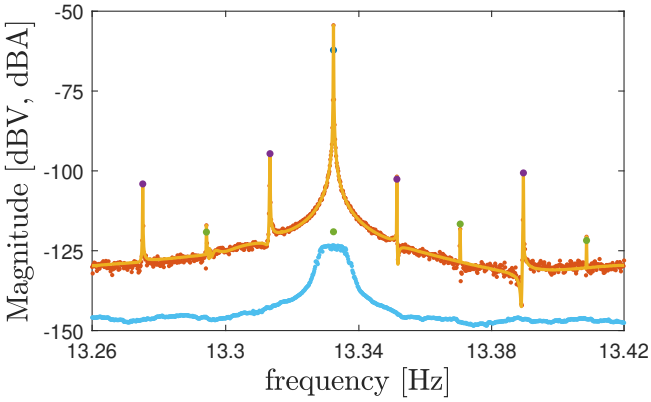

Fig. 13. Zoomed input-output spectrum of the system. Blue: $U(f)$, red: $Y(f)$, yellow: $\hat{Y}(f)$, purple: $\hat{\sigma}^2_{Y_{\mathrm{s,even},0}}(f)$, green: $\hat{\sigma}^2_{Y_{\mathrm{s,odd},0}}(f)$ and light blue: $\hat{\sigma}^2_V(f)$.

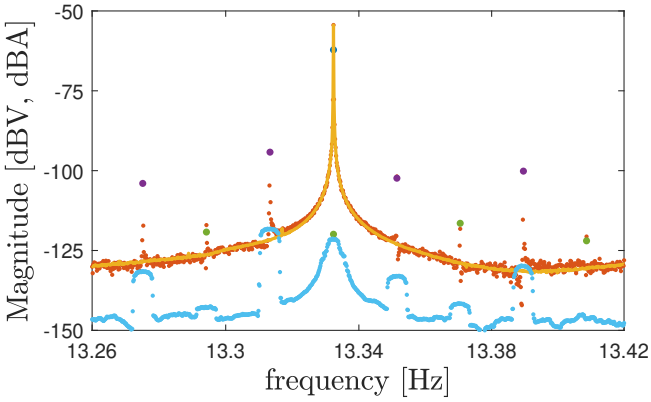

Fig. 14. Method from [22] applied to the corrosion measurement. Blue: $U(f)$, red: $Y(f)$, yellow: $\hat{Y}(f)$, purple: $\hat{\sigma}^2_{Y_{\mathrm{s,even}}}(f)$, green: $\hat{\sigma}^2_{Y_{\mathrm{s,odd}}}(f)$ and light blue: $\hat{\sigma}^2_V(f)$.

IX. Measurement Example II

In order to show that the methods detailed in this paper are applicable to a large class of systems/processes, we apply it to a second measurement example here.

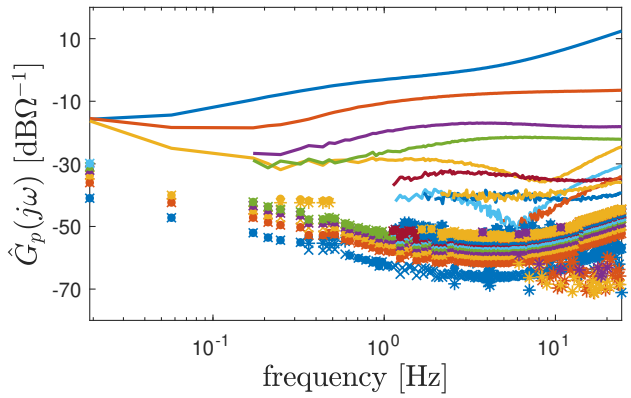

Fig. 15. Estimated BLA's of the block schematic with their uncertainties. Full lines: $\hat{G}_p(j\omega)$, dots: total variance, crosses: variance due to noise and stars: variance due to odd nonlinear distortions. Colors for $p = 0, 1..., 9$: blue, red, yellow, purple, green, light blue, bordeaux, blue, red and yellow.

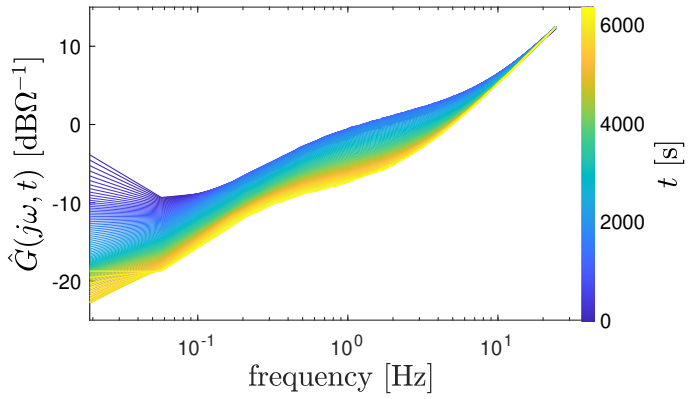

Fig. 16. Magnitude of the estimated time-varying admittance $\hat{G}(j\omega, t)$ of the pitting corrosion measurement.

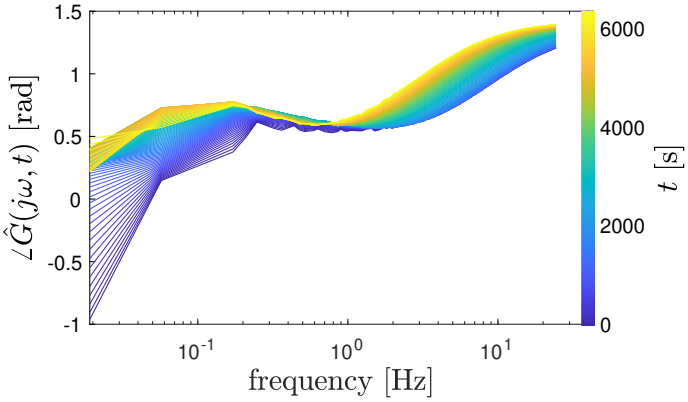

Fig. 17. Phase of the estimated time-varying admittance $\hat{G}(j\omega, t)$ of the pitting corrosion measurement.

In this measurement example, the electrorefining of copper is studied. The system consists of a copper rotating disc working electrode, a calomel reference electrode with K_2SO_4 salt bridge and a Pt counter electrode. The electrolyte that is used mimics the conditions in the electrorefining process. It consists of 0.6M $CuSO_4$, 2M H_2SO_4, ppm level chlorides and with thiourea as additive.

A current is applied to the process and the voltage between working and reference electrode is measured. The excitation signal is the sum of a constant current of $-5.6\,\text{mA}$, which is applied for the electrodeposition of Cu, and an odd random phase multisine of $0.5\,\text{mA}$ RMS, exciting 384 frequencies in the band $[5\,\text{mHz}, 15\,\text{kHz}]$ and with a period length $T_p = 200\,\text{s}$. Note that the band of interest is as wide as 6 decades. Both current and voltage signals were measured for $P = 29$ periods of the multisine, corresponding to a measurement time $T = 5800\,\text{s}$, at a sampling rate $f_s = 45\,\text{kHz}$. This was done using an NI PCI-4461 data acquisition card, connected to a custom-built compact analog potentiostat and with in-house developed software. The input-output spectrum is shown in Fig. 18. Note the presence of a trend in the output spectrum. The algorithms of Sections III and IV are applied with hyper parameters $N_q = 5$, $N_p = 7$, $N_a = 8$ and dof $= 5$ in (42) and (58). This results in a local bandwidth of $2n + 1 = 49$ (8.4 mHz). For the noise estimation, the number of nonzero singular values m varies over frequency between 9 and 20 while $n_\theta = 28$ or 35. The estimates of the even and odd stationary nonlinear distortions, and the noise level are shown in Fig. 18. Note the peak in the noise estimate around the European mains frequency of 50 Hz. The estimates of the time-varying nonlinear distortions are not shown for the sake of clarity. Even and odd nonlinear distortions are detected, quantified and classified. Also in this measurement, the even nonlinear distortions are the strongest ones. A zoomed version of the input-output spectrum is shown in Fig. 19. Here, it is also clearly visible that skirts are present around all integer multiples of the fundamental frequency $f_0 = 5\,\text{mHz}$, and, hence, time-varying nonlinearities are present. Note that the noise estimate is higher around the excited frequencies, which can be explained by nonlinear process noise – input signal interactions in the copper electrorefining dynamics.

The LTI transfer function blocks are shown in Fig. 20 together with their uncertainties due to noise, nonlinear distortions and both. Finally the time-varying impedance of the electrorefining process is shown in Figs. 21 and 22. The uncertainties of the time-varying impedance are not shown for reasons of clarity.

X. Conclusions

In this paper a method has been detailed for obtaining linear models for nonlinear time-varying systems. This under the form of a time-varying transfer function. A linear model for a nonlinear system is only justifiable when the nonlinear distortions are not too strong with regard to the linear part of the system for a given application. Hence, in the measurement, the time-varying nonlinear distortions must be detected and quantified. Moreover, nonlinear distortions could be classified between even and odd ones, giving more insight about

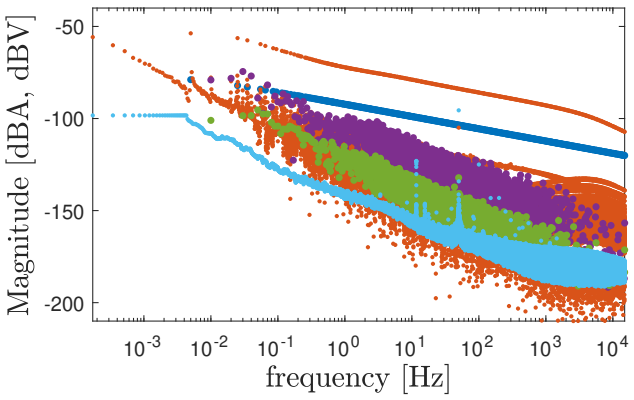

Fig. 18. Input-output spectrum of the copper electrorefining process measurement. Blue: $U(f)$, red: $Y(f)$, purple: $\hat{\sigma}^2_{Y_{s,even,0}}(f)$, green: $\hat{\sigma}^2_{Y_{s,odd,0}}(f)$ and light blue: $\hat{\sigma}^2_V(f)$.

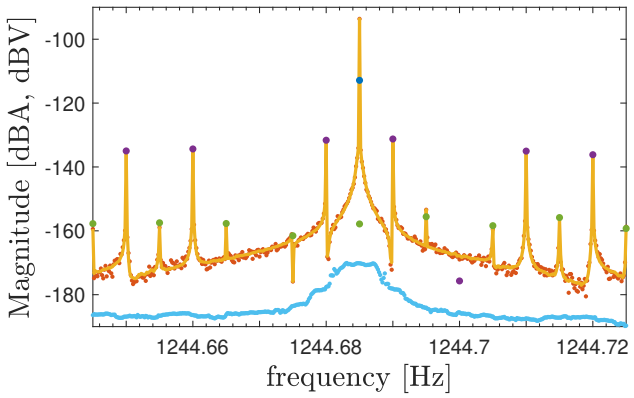

Fig. 19. Zoomed input-output spectrum of the copper electrorefining process measurement. Blue: $U(f)$, red: $Y(f)$, yellow: $\hat{Y}(f)$, purple: $\hat{\sigma}^2_{Y_{s,even,0}}(f)$, green: $\hat{\sigma}^2_{Y_{s,odd,0}}(f)$ and light blue: $\hat{\sigma}^2_V(f)$.

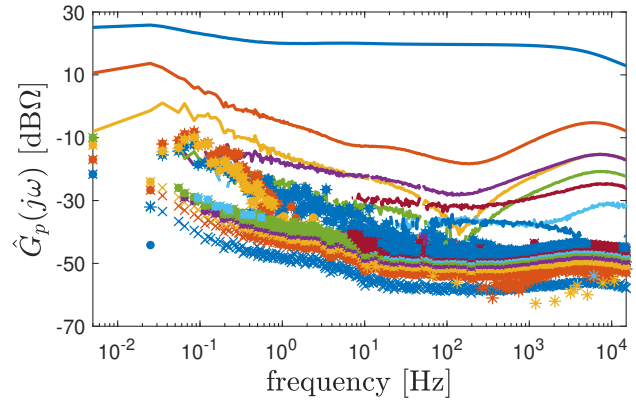

Fig. 20. Estimated BLA's of the block schematic with their uncertainties for the copper electrorefining process measurement. Full lines: $\hat{G}_p(j\omega)$, dots: total variance, crosses: variance due to noise and stars: variance due to odd nonlinear distortions. Colors for $p = 0, 1..., 7$: blue, red, yellow, purple, green, light blue, bordeaux and blue.

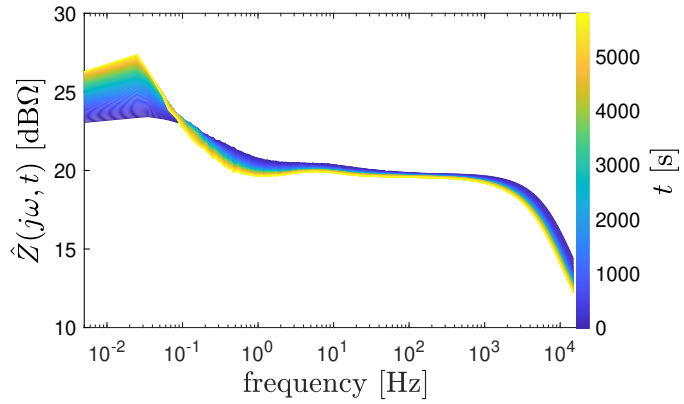

Fig. 21. Magnitude of the estimated time-varying impedance $\hat{Z}(j\omega, t)$ of the copper electrorefining process measurement.

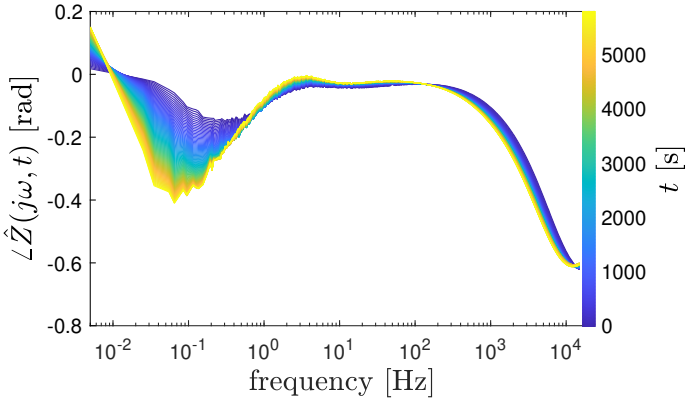

Fig. 22. Phase of the estimated time-varying impedance $\hat{Z}(j\omega, t)$ of the copper electrorefining process measurement.

the system. Also uncertainty bounds were computed on the nonparametric values of the TV-FRF, this due to nonlinear distortions, noise and both. The identification technique of this paper is applicable to a large class of systems, where the method of [22] would fail. Additionally, trends and noise are allowed in the measurements. Furthermore, very large frequency bands of interest can be studied.

For making the identification technique more accessible, algorithms were developed were the user only has to choose upper bounds on a number of hyper parameters defining the model structure.

The algorithms have been validated on a Monte-Carlo simulation and applied to measurements of two real-life examples.

APPENDIX

For linear time-varying systems, a trend can only be introduced when the excitation signal has a non-zero mean. For the time-invariant branch, a trend is caused when the transfer function $G_0(s)$ has one or more poles at the origin. For the time-varying branches, however, it is sufficient that $G_p(s)$, $p \geqslant 1$, has a non-zero DC gain, as the output of this dynamical system is multiplied by the basis function $b_p(t)$. Hence, for LTV systems, the sufficient conditions for a trend are that the

input signal has a non-zero mean and that the time-invariant transfer function has one or more poles at the origin, or at least one of the time-varying branches has a non-zero DC gain.
For the class of systems considered, see Definition 2 and Fig. 2, a trend can be present even if the system is excited by a zero-mean input signal. This trend can be formed in different ways. For instance, assuming that the blocks NL_p are Wiener-Hammerstein systems, see Fig. 7, an even nonlinear part of the function $f_p^1(x)$ introduces a DC value in the signal that is fed to $H_p(s)$. Hence if $H_p(s)$ has one or more poles at the origin for $p = 0$ or has a finite non-zero DC gain for $p \geqslant 1$, a trend can be present. Hence in this case the necessary conditions are that (i) an even nonlinearity is present in one or more branches, and (ii) in these branches $H_p(s)$ has poles at the origin for $p = 0$ or has a non-zero DC gain for $p \geqslant 1$.
The term $y_{\text{trend}}(t)$ in (17) stands for the trend created by all this mechanisms, as nonparametric models of the transfer functions $G_p(s)$ cannot contain the information about the trend.

REFERENCES

[1] L. Ljung, *System Identification: Theory for the User*. Prentice Hall, 1999.

[2] R. Pintelon and J. Schoukens, *System identification: a frequency domain approach*. John Wiley & Sons, 2012.

[3] Y. Rolain, W. Van Moer, R. Pintelon, and J. Schoukens, "Experimental characterization of the nonlinear behavior of rf amplifiers," *IEEE transactions on microwave theory and techniques*, vol. 54, no. 8, pp. 3209–3218, 2006.

[4] E. Wernholt and S. Gunnarsson, "Estimation of nonlinear effects in frequency domain identification of industrial robots," *IEEE Transactions on instrumentation and measurement*, vol. 57, no. 4, pp. 856–863, 2008.

[5] M. Schoukens and K. Tiels, "Identification of block-oriented nonlinear systems starting from linear approximations: A survey," *Automatica*, vol. 85, pp. 272–292, 2017.

[6] J. Schoukens, R. Pintelon, T. Dobrowiecki, and Y. Rolain, "Identification of linear systems with nonlinear distortions," *Automatica*, vol. 41, no. 3, pp. 491–504, 2005.

[7] M. Schoukens, R. Pintelon, T. P. Dobrowiecki, and J. Schoukens, "Extending the best linear approximation framework to the process noise case," *IEEE Transactions on Automatic Control*, vol. 65, no. 4, pp. 1514–1524, 2019.

[8] R. Pintelon, M. Schoukens, and J. Lataire, "Best linear approximation of nonlinear continuous-time systems subject to process noise and operating in feedback," *IEEE Transactions on Instrumentation and Measurement*, 2020.

[9] M. Moltedo, G. Cavallo, T. Baček, J. Lataire, B. Vanderborght, D. Lefeber, and C. Rodriguez-Guerrero, "Variable stiffness ankle actuator for use in robotic-assisted walking: Control strategy and experimental characterization," *Mechanism and Machine Theory*, vol. 134, pp. 604–624, 2019.

[10] X. Zhu, L. F. Macía, J. Jaguemont, J. de Hoog, A. Nikolian, N. Omar, and A. Hubin, "Electrochemical impedance study of commercial lini0. 80co0. 15al0. 05o2 electrodes as a function of state of charge and aging," *Electrochimica Acta*, vol. 287, pp. 10–20, 2018.

[11] L. A. Zadeh, "Frequency analysis of variable networks," *Proceedings of the IRE*, vol. 38, no. 3, pp. 291–299, 1950.

[12] J. Lataire, R. Pintelon, and E. Louarroudi, "Non-parametric estimate of the system function of a time-varying system," *Automatica*, vol. 48, no. 4, pp. 666–672, 2012.

[13] N. Hallemans, J. Lataire, and R. Pintelon, "Nonparametric identification of linear time-varying systems using gaussian process regression," *IFAC-PapersOnLine*, vol. 53, no. 2, pp. 1001–1006, 2020.

[14] M. E. Orazem and B. Tribollet, *Electrochemical impedance spectroscopy*. John Wiley & Sons, 2008.

[15] A. Battistel, G. Du, and F. La Mantia, "On the analysis of non-stationary impedance spectra," *Electroanalysis*, vol. 28, no. 10, pp. 2346–2353, 2016.

[16] D. Koster, G. Du, A. Battistel, and F. La Mantia, "Dynamic impedance spectroscopy using dynamic multi-frequency analysis: A theoretical and experimental investigation," *Electrochimica Acta*, vol. 246, pp. 553–563, 2017.

[17] A. Battistel and F. La Mantia, "On the physical definition of dynamic impedance: How to design an optimal strategy for data extraction," *Electrochimica Acta*, vol. 304, pp. 513–520, 2019.

[18] T. Holm, P. K. Dahlstrøm, S. Sunde, F. Seland, and D. A. Harrington, "Dynamic electrochemical impedance study of methanol oxidation at pt at elevated temperatures," *Electrochimica Acta*, vol. 295, pp. 139–147, 2019.

[19] E. Van Gheem, R. Pintelon, A. Hubin, J. Schoukens, P. Verboven, O. Blajiev, and J. Vereecken, "Electrochemical impedance spectroscopy in the presence of non-linear distortions and non-stationary behaviour: Part ii. application to crystallographic pitting corrosion of aluminium," *Electrochimica acta*, vol. 51, no. 8-9, pp. 1443–1452, 2006.

[20] E. Van Gheem, R. Pintelon, J. Vereecken, J. Schoukens, A. Hubin, P. Verboven, and O. Blajiev, "Electrochemical impedance spectroscopy in the presence of non-linear distortions and non-stationary behaviour: Part i: Theory and validation," *Electrochimica Acta*, vol. 49, no. 26, pp. 4753–4762, 2004.

[21] R. Pintelon, E. Louarroudi, and J. Lataire, "Time-variant frequency response function measurements on weakly nonlinear, arbitrarily time-varying systems excited by periodic inputs," *IEEE Transactions on Instrumentation and Measurement*, vol. 64, no. 10, pp. 2829–2837, 2015.

[22] N. Hallemans, R. Pintelon, X. Zhu, T. Collet, R. Claessens, B. Wouters, A. Hubin, and J. Lataire, "Detection, classification, and quantification of nonlinear distortions in time-varying frequency response function measurements," *IEEE Transactions on Instrumentation and Measurement*, vol. 70, pp. 1–14, 2021.

Noël Hallemans was born in Brussels, Belgium, in 1996. He obtained his master's degree in electrical engineering in 2019 from the Vrije Universiteit Brussel (VUB) and Université Libre de Bruxelles (ULB). Since September 2019 he has been working as a researcher with the ELEC department, VUB, Brussels. His research focuses on data-driven modelling, including linear approximations and kernel-based regression.

Rik Pintelon (M'90-SM'96-F'98) was born in Gent, Belgium, on December 4, 1959. He received a master's degree in electrical engineering in 1982, a doctorate (Ph.D) in engineering in 1988, and the qualification to teach at university level (geaggregeerde voor het hoger onderwijs) in 1994, all from the Vrije Universiteit Brussel (VUB), Brussels, Belgium. In 2014 he received the degree of Doctor of Science (DSc) from the University of Warwick (UK) for publications with the collective title "Frequency Domain System Identification: A Mature Modeling Tool". From 1982 to 1984 and 1986 to 2000, Dr. Pintelon was a researcher with the Belgian National Fund for Scientific Research (FWO-Vlaanderen) at the Electrical Engineering (ELEC) Department of the VUB. From 1984 to 1986 he did his military service overseas in Tunesia at the Institut National Agronomique de Tunis. From 1991 to 2000 he was a part-time lecturer at the department ELEC of the VUB, and since 2000 he is a full-time professor in electrical engineering at the same department. From 2009 to 2018 he was a visiting professor at the department of Computer Sciences of the Katholieke Universiteit Leuven, and from 2013 to 2018 he was a honorary professor in the School of Engineering of the University of Warwick. His main research interests include system identification, signal processing, and measurement techniques. Dr. Pintelon is the coauthor of 4 books on System Identification and the coauthor of more than 260 articles in refereed international journals. He has been a Fellow of IEEE since 1998. Dr. Pintelon was the recipient of the 2012 IEEE Joseph F. Keithley Award in Instrumentation and Measurement (IEEE Technical Field Award). He received the 2008 IOP outstanding paper award (best paper in Measurement Science & Technology), the 2014 Martin Black prize (best paper in Physiological Measurement) and the 2014 Andy Chi award (best paper in IEEE Trans. on Instrumentation and Measurement).

John Lataire (S'06-M'11) was born in Brussels, Belgium, in 1983. He received the Electrical Engineer degree in electronics and information processing and the Ph.D. degree in engineering sciences (Doctor in de Ingenieurswetenschappen) from the Vrije Universiteit Brussel, Brussels, in 2006 and 2011, respectively. From October 2007 to October 2011, he was on a Ph.D. fellowship from the Research Foundation—Flanders (FWO). Since August 2006, he has been working as a Researcher with the Department ELEC-VUB, Brussels. Dr. Lataire is the coauthor of more than 30 articles in refereed international journals. He received the 2008 IOP outstanding paper award (best paper in Measurement Science & Technology), the Best Junior Presentation Award 2010 at the 29th Benelux Meeting on Systems and Control, was the co-recipient of the 2014 Andy Chi award (best paper in IEEE Trans. on Instrumentation and Measurement), and was the recipient of the 2016 J. Barry Oakes Advancement Award (from the IEEE Instrumentation and Measurement society). His main interests include the frequency domain formulation of the identification of dynamic systems, with a specific focus on the identification of time-varying systems, and the use of kernel-based regression in system identification.

Els Van Gheem was born in Brasschaat, in 1975. She obtained her master's degree in chemical engineering in 1998 and her PhD in Applied Sciences in 2005, both from the Vrije Universiteit Brussel (VUB). Her research focused on the non-linear and non-stationary behavior of pitting corrosion of Aluminum. Besides the in depth electrochemical research, the PhD also demonstrated how a proven methodology from electronics can be transferred to materials science.

Thomas Collet received a master's degree in Applied Engineering from the University of Antwerp in 2014 and a master's degree in Chemical and Materials Engineering from the Vrije Universiteit Brussel in 2016. Since 2017, he has been working on a PhD in collaboration with Aurubis Belgium and with the support of Flanders Innovation & Entrepreneurship (VLAIO) to study the copper electrorefining process.

Benny Wouters obtained his Industrial Engineer degree in chemistry from the Artesis University college Antwerp in 2010 and his joint Ph.D. degree in Engineering Sciences and Applied Engineering from the Vrije Universiteit Brussel and the University of Antwerp in 2016. Since 2016 he is working as a postdoc researcher in the Electrochemical and Surface Engineering (SURF) research group at VUB. His research focuses on advanced Electrochemical Impedance Spectroscopy in the fields of corrosion protection, batteries and electrochemical processing.

Raf Claessens received a master's degree in Applied Engineering from UC Limburg (1992); and a postgraduate in Computer Sciences (1996) and a Master of Science in Electrical Engineering (2002) from the Catholic University of Leuven (KU Leuven). From 2006 on he has been working with the VUB Materials and Chemistry research group on advanced thermal analysis, X-ray diffraction and impedance spectroscopy research projects.

Annick Hubin is professor at the Faculty of Engineering of the Vrije Universiteit Brussel, Belgium. She is head of the Research Group Electrochemical and Surface Engineering. Her research is situated in the field of electrochemical engineering with a strong focus on electrochemical system identification. Applications are among others in electrodeposition, electrocatalysis, corrosion, batteries.

Kristof Ramharter received a master's degree in Materials Engineering from the University of Leuven in 2016 and a master's degree in Management from the University of Leuven in 2017. From 2017 until 2018, he was solving corrosion issues for SUEZ WTS in Europe, Middle-East and Africa. Since 2018, he has been working as Jr. R&D Manager at Aurubis Belgium. His research mostly focuses on hydrometallurgical – but also pyrometallurgical – refining of copper and recycling technologies that are linked with those flowsheets.